TU Delft

Delft University of Technology

Document Version
Final published version

Licence
Dutch Copyright Act (Article 25fa)

Citation (APA)
Liang, H., Tang, Z., Chen, Z., Zhao, Z., Zeng, M., Gong, W., Wang, F., French, P. J., Wang, Q., & More Authors (2026). Hollow 3D PANI@PSS-rGO microspheres enabling ultra-sensitive room temperature ammonia gas sensing. *Sensors and Actuators B: Chemical*, *460*, Article 139955. https://doi.org/10.1016/j.snb.2026.139955

Important note
To cite this publication, please use the final published version (if applicable).
Please check the document version above.

Copyright
In case the licence states “Dutch Copyright Act (Article 25fa)”, this publication was made available Green Open Access via the TU Delft Institutional Repository pursuant to Dutch Copyright Act (Article 25fa, the Taverne amendment). This provision does not affect copyright ownership.
Unless copyright is transferred by contract or statute, it remains with the copyright holder.

Sharing and reuse
Other than for strictly personal use, it is not permitted to download, forward or distribute the text or part of it, without the consent of the author(s) and/or copyright holder(s), unless the work is under an open content license such as Creative Commons.

Takedown policy
Please contact us and provide details if you believe this document breaches copyrights.
We will remove access to the work immediately and investigate your claim.

This work is downloaded from Delft University of Technology.

Sensors & Actuators: B. Chemical 460 (2026) 139955



Contents lists available at ScienceDirect

Sensors and Actuators: B. Chemical

journal homepage: www.elsevier.com/locate/snb





Hollow 3D PANI@PSS-rGO microspheres enabling ultra-sensitive room temperature ammonia gas sensing

Hongping Liang [a,b], Zilun Tang [b], Zhuo Chen [c], Zhenting Zhao [b], Min Zeng [d], Weiping Gong [b,*], Fei Wang [e], Patrick J. French [f], Quan Wang [a], Hao Li [a], Guofu Zhou [a], Yao Wang [a,*]

[a] Guangdong Provincial Key Laboratory of Optical Information Materials and Technology & Institute of Electronic Paper Displays, South China Academy of Advanced Optoelectronics, National Center for International Research on Green Optoelectronics, South China Normal University, Guangzhou 510006, China
[b] Guangdong Provincial Key Laboratory of Electronic Functional Materials and Devices, Huizhou University, Huizhou 516007, China
[c] Physical Sciences and Engineering Division, King Abdullah University of Science and Technology (KAUST), Thuwal 23955−6900, Saudi Arabia
[d] National Key Laboratory of Advanced Micro and Nano Manufacture Technology, Shanghai Jiao Tong University, Shanghai 200240, China
[e] School of Microelectronics, Southern University of Science and Technology, Shenzhen 518055, China
[f] BE Lab, Faculty EWI, Delft University of Technology, Delft 2628CD, the Netherlands

ARTICLE INFO

Dataset link: Raw sensing data and calibration datasets

Keywords:
Hollow sphere
Graphene
Polyaniline
Ammonia sensing
Room temperature

ABSTRACT

Designing sensing materials with distinct morphologies remains a key challenge in the development of high-performance gas-sensing devices. In this study, we employed a supramolecular assembly and ice-melting-induced lyophilization (IMIL) technique to synthesize poly (sodium p-styrenesulfonate)-functionalized reduced graphene oxide (PSS-rGO) microspheres. We then used in situ chemical oxidation polymerization to create a hollow three-dimensional (3D) polyaniline-decorated PSS-rGO microspheres (PANI@PSS-rGO) and conducted a trace analysis of ammonia (NH_3) at room temperature. The PANI was uniformly decorated on the surfaces of the PSS-rGO microspheres, and the PANI@PSS-rGO exhibited a hollow microsphere morphology. This structure's large specific surface area provided sufficient adsorption sites and enabled fast multichannel charge transfer. The hollow 3D PANI@PSS-rGO composite had ultra-high sensitivity of 7.06% / ppm at high concentrations and 55.86% / ppm at low concentrations, as well as short response and recovery times of 9 and 120 s, respectively. We attributed the good selectivity, repeatability, and long-term stability of the PANI@PSS-rGO composite to the significant synergistic effect of the PANI and the PSS-rGO. We determined a promising route to room-temperature gas sensors for ultrasensitive trace analysis of NH_3, which is enabled by this 3D framework.

1. Introduction

One of the most prominent pollutants well known for causing serious health effects is ammonia (NH_3). These health problems include irritation of the eye, skin, respiratory tract irritation, as well as dizziness and nausea [1,2]. A biomarker for non-invasive clinical diagnosis of kidney and liver disease is human-exhaled NH_3 as a product of protein respiration [3,4]. The exhaled NH_3 concentration of healthy individuals is typically less than 0.96 parts per million (ppm), with a range of 0.425–1.8 ppm, and that of nephrotic patients is approximately 4.88 ppm, with a range of 0.82–14.7 ppm [5]. Developing gas sensors with high sensitivity to NH_3 at room temperature is critical for human health monitoring. Today, numerous materials are being used to fabricate NH_3 sensors, including metal oxide semiconductors (MOS) [6], MXenes[7], graphene [8,9], conducting polymers [10], and their composites [11,12].

Conducting polymers including polyaniline (PANI) [13], polypyrrole (PPy) [14], and polythiophene (PTh) [15] exhibit sensitivity at room temperature, and their physical and chemical properties can be simultaneously tuned by using different substituents [16]. PANI is one of the most popular conducting polymers used in NH_3 sensing because of its flexibility, processability, good conductivity, doping and dedoping chemical reaction, good environmental stability, and reactivity with NH_3[17]. However, the aggregation and disorder of PANI result in long response and recovery times for sensors. Consequently, significant efforts have been invested in fabricating highly ordered PANI. For

* Corresponding authors.
E-mail addresses: gwp@hzu.edu.cn (W. Gong), wangyao@m.scnu.edu.cn (Y. Wang).

https://doi.org/10.1016/j.snb.2026.139955
Received 28 October 2025; Received in revised form 30 March 2026; Accepted 8 April 2026
Available online 9 April 2026
0925-4005/© 2026 Elsevier B.V. All rights are reserved, including those for text and data mining, AI training, and similar technologies.

example, highly ordered polyaniline thin films were synthesized at an air-water interface using a template-free method [18]. However, these sensors continue to suffer from low sensitivity and prolonged response and recovery times due to the low specific surface area of 2D polyaniline.

Because of graphene's excellent electrical conductivity and large specific surface area (2630 m^2g^{-1}), it is an appealing gas-sensing material [19]. In recent years, extensive efforts have been devoted to developing gas sensors based on graphene and its derivatives [20]. However, pure graphene has poor gas-sensing performance because its strong π–π stacking causes self-aggregation [21]. Incorporating other sensing materials (e.g., metals, metal oxides, and conducting polymers) into graphene sheets effectively prevents agglomeration and achieves suitable nanostructure distribution, which is crucial for enhancing sensor performance [22,23]. In our recent work, we assembled Pt nanoparticles onto 2D graphene sheets, transforming them into hollow three-dimensional (3D) structures using the ice-melting-induced lyophilization (IMIL) technique. These Pt-decorated graphene spheres demonstrated an ultralow limit of detection (LOD) and ultrafast response and recovery speed for room-temperature formaldehyde sensing due to their increased gas adsorption capabilities [24].

Researchers have fabricated graphene/PANI composites with good sensing performance by combining the sensing properties of both graphene and PANI [22,25,26]. By decorating graphene with PANI, the recombination rate of electron–hole pairs can be slowed down through π–π interactions, and the charge transfer rate of electrons can be increased [16]. Nevertheless, their sensitivity, response/recovery speed, and stability are still unsatisfactory, which may be due to the inhibition of NH_3 adsorption by structural disorder [10,27]. In gas-sensing applications, considerable attention has recently been given to graphene-based materials with various structures and morphologies [28,29]. Sufficient active sites to absorb NH_3 have been identified in 3D graphene-based materials with large specific surface areas [30]. Template methods have been developed to avoid the agglomeration of 3D PANI [31,32]. For example, the construction of three-dimensional PANI@rGO@SiO_2 composites relies on SiO_2 nanoparticles, which reduce the number of active sites [33]. Hollow 3D PANI microspheres with good conductivity can be obtained by dissolving the polystyrene spheres sacrificial template [34]. However, template-removal steps increase the complexity of the fabrication process and risk damaging the structural integrity of the composite, thereby compromising its sensing performance. How to achieve ultra-sensitive and ultra-stable PANI-based sensor without template removal is technically challenging. Therefore, we demonstrate the in-situ polymerization of PANI on poly (sodium p-styrenesulfonate)-functionalized reduced graphene oxide (PSS-rGO) microspheres without using sacrificial templates.

In this study, we used an in situ chemical oxidation polymerization method to obtain the hollow 3D PANI-decorated poly (sodium p-styrenesulfonate)-functionalized reduced graphene oxide (PANI@PSS-rGO) microspheres for trace NH_3 detection at room temperature. Our work realizes the facile synthesis of graphene/PANI composites with good structural integrity and abundant NH_3 adsorption sites by adopting PSS-rGO microspheres, thereby eliminating the need for sacrificial templates and enhancing the sensing performance. The obtained PANI@PSS-rGO microspheres exhibited a high response (643%) to 50 ppm of NH_3 with short response and recovery times of 9 and 120 s, respectively. The microspheres also exhibited good selectivity, outstanding repeatability, and stable long-term performance. The sensor also showed detectable sensitivity to NH_3 with a response value of 7% at low concentrations of 10 parts per billion (ppb). The ability to achieve stable monitoring of low concentrations of NH_3 is essential for disease diagnosis and environmental applications.

2. Experimental section

2.1. Materials

We purchased poly (sodium p-styrenesulfonate) (PSS, ≥99%, M_w = 80000) and hydrazine hydrate ($N_2H_4{\cdot}H_2O$, ≥80%) from Alfa Aesar (Shanghai, China). We obtained graphite from XianFeng NANO Co., Ltd. (Nanjing, China). We obtained Millipore filters (0.22 μm, nylon) from Shanghai Titan Scientific Co., Ltd. (Shanghai, P. R. China). We obtained and used as received ammonium persulfate (APS, ≥98%), aniline monomer (ANI, ≥99.5%), and hydrochloric acid (HCl, ≥37%) from Sigma-Aldrich (St. Louis, MO, USA). We purchased acetic acid ($C_2H_4O_2$, ≥99.5%), acetone (C_3H_6O, ≥99.5%), ethanol (C_2H_6O, ≥99.7%), formaldehyde (CH_2O, ≥37%), and methanol (CH_4O, 99.5%) from Tianjin Zhiyuan Chemical Reagent Co., Ltd. (Tianjin, China). We used all other chemical reagents, which were analytically pure, without further purification.

2.2. PSS-functionalized graphene microspheres preparation

We followed a modified Hummers' method to prepare the GO [35]. We used supramolecular assembly and ice-melting-induced lyophilization technique to prepare the PSS-functionalized graphene microspheres. We added graphene oxide (30 mL, 0.3 mg/mL) and poly (sodium p-styrenesulfonate) (180 mg) to a flask. We stirred for 10 min and then added hydrazine hydrate (20 mL, 1.12 μL/mL). We maintained the reactant for 1 h at 80°C. The resulting products were rinsed 3 times with deionized water and redispersed into 30 mL of deionized water to obtain PSS-rGO dispersion. We used vertical immersion in liquid nitrogen for 5 min to solid freeze the PSS-rGO dispersion, which we moved to an oven and maintained for 6 min at 60°C. We transferred the product to a lyophilizer for 48 h under 20 Pa at about −40°C to obtain the PSS-rGO microspheres [24].

2.3. Sensing materials preparation

The PANI@PSS-rGO composites were prepared via an in situ chemical oxidation polymerization method. The optimal PANI@PSS-rGO microspheres were obtained by optimizing the polymerization time and adjusting the weight ratio of aniline to PSS-rGO microspheres. The polymerization time was set to 1, 3, 5, 7, and 18 h to explore the optimal polymerization time. 90, 40, 20, 10, 5, 2.5, and 1.1 mg of the obtained PSS-rGO microspheres were dispersed separately in 10 mL of hydrochloric acid solution (1 M). We added 10 μL of aniline to the dispersion and then provided mild sonication for 30 min. After we transferred the mixed solution to a refrigerator at 4°C, 50 mg of ammonium persulfate (APS) was added. After 3-h polymerization process, we washed the products three times with deionized water and then we lyophilized the product and obtained the PANI@PSS-rGO composites. The as-obtained samples were labelled as PANI@PSS-rGO-90, PANI@PSS-rGO-80, PANI@PSS-rGO-66, PANI@PSS-rGO-50, PANI@PSS-rGO-33, PANI@PSS-rGO-20, and PANI@PSS-rGO-10, which had PSS-rGO weight ratios of 90%, 80%, 66%, 50%, 33%, 20%, and 10%, respectively. PANI@PSS-rGO-X denotes composites containing X wt% of PSS-rGO relative to the theoretical total mass of the composite. For comparison, we simultaneously prepared PANI/PSS-rGO and PANI/rGO using PSS-rGO and reduced graphene oxide (rGO) nanosheets, respectively.

2.4. Gas-sensing measurements

Drop-dry method was used to prepare the sensors. First, the as-obtained sensing materials were initially redispersed into deionized water to form a dispersion (1 mg/mL). Then, 20 μL of dispersion was uniformly deposited onto the ceramic substrate's Ag-Pd interdigital electrodes (IDEs), with the electrode gap and finger width of 200 μm. Finally, to prepare for the next round of tests, we dried the gas sensors

for 5 min on a heater at 60°C. All sensing measurements were specifically performed using a gas and liquid distribution system (DGL-III, Beijing Elite Technology Co., Ltd.) equipped with mass flow controllers (MFCs) (Scheme 1). Certified 100% NH_3 gas was diluted to the required ppm levels using dry air as the carrier gas at a flow rate of 200 sccm. Certified 1000 ppm NH_3 gas was used to obtain the required ppb levels of NH_3. The relative humidity (RH) was controlled by passing dry air through the bubble chamber. The gas sensor was placed in a 10 mL test chamber and exposed to various concentrations of NH_3. The real-time resistance changes in the sensors were monitored using an electrometer (Keithley 2450). After each 2-minute NH_3 exposure, the chamber was purged with dry air for 3 min to restore the sensor baseline. Unless otherwise specified, all sensor tests were conducted at room temperature (25 ± 2 °C) and a relative humidity of 30 ± 2%. For the volatile organic compounds (VOCs), including formaldehyde, acetic acid, ethanol, acetone, and methanol, their vapors were produced by heating each corresponding compound using a heating plate within the system. The relationship between the volume of the corresponding liquid and the gas concentration is given in Eq. (1).

$$Q = \frac{V \times C \times M}{22.4 \times d \times p} \times \frac{273 + T}{273 + T_c} \quad (1)$$

Where Q (mL) is the volume of liquid, V (L) denotes the testing chamber volume, C denotes the gas concentration, M (g/mol) denotes the molecular weight of target gas, d (g/cm^3) represents the density of the liquid, p represents the purity of the liquid, T (°C) represents the ambient temperature, and T_c (°C) represents the temperature inside the testing chamber.

Eq. (2) shows the calculation of the gas sensor's response:

$$\text{Response}\ (\%) = (R_g - R_a)/R_a \times 100\% = \Delta R / R_a \times 100\% \quad (2)$$

where the resistance value of the sensor in air is R_a and the resistance value of the sensor in NH_3 is R_g.

The response time is defined as the time required for the sensor resistance to reach 90% of the total saturation value (T_{90}) upon gas injection. The recovery time is defined as the time required for the sensor resistance to recover 90% of its baseline value after gas removal. The practical limit of detection (pLOD) is defined as the lowest concentration of NH_3 detectable in ambient air throughout the experiment.

2.5. Characterization

The samples were examined using Fourier transform infrared spectroscopy (FTIR; Bruker Vertex 70, Karlsruhe, Germany) and Raman scattering spectroscopy (inVia; Renishaw, Wooten-under-Edge, UK) equipped with a 530-nm laser. The surface elemental composition analysis of PANI and PANI@PSS-rGO-80 microspheres was studied using X-ray photoelectron spectroscopy (XPS, Escalab 250Xi; Thermo-Fisher, Waltham, MA, USA) in a vacuum of less than 5.0×10^{-10} mBa. For reference, the C1S peak was set at 284.8 eV. We used field emission scanning electron microscopy (FESEM, FEI Quanta 250 FEG) to evaluate the morphologies of PANI, the PANI@PSS-rGO composites, and the PSS-rGO microspheres. To verify the uniform coverage of PANI on the PANI@PSS-rGO-80 microspheres and of PSS on the PSS-rGO microspheres, we conducted field emission scanning electron microscopy (FESEM, ZEISS Ultra 55; Oberkochen, Germany) with energy dispersive X-ray spectroscopy mapping (EDS mapping). Transmission electron microscopy (TEM, JEM-1400 PLUS; JEOL, Tokyo, Japan) was employed to characterize the morphological structure of the PANI@PSS-rGO-80 microspheres.

3. Results and discussion

3.1. Structural and morphological characterization

Fig. 1 shows the preparation method of the sensing materials. First, PSS was supramolecularly assembled with graphene oxide through π–π interactions. Second, hollow 3D PSS-rGO microspheres were constructed using the IMIL technique. Finally, in situ chemical oxidation polymerization was then employed to construct hollow 3D PANI@PSS-rGO microspheres. As shown in Fig. 2, the structural characteristics and functional groups of the materials were characterized using FTIR and Raman spectroscopy. Fig. 2a shows the FTIR spectra of GO, PSS, PSS-rGO, PANI@PSS-rGO-80, and pure PANI microspheres. The PSS spectrum exhibited absorption peaks at around 1647 cm^{-1}, 1414 cm^{-1}, and 1194–1008 cm^{-1}. These peaks corresponded to the benzene ring absorption, the C–C vibration band, and the S = O stretching vibration of the PSS carbon skeleton. The PSS-rGO spectrum exhibited absorption peaks at 2853 cm^{-1}, which corresponded to the symmetric stretching, and at 2922 cm^{-1}, which corresponded to the asymmetric stretching of

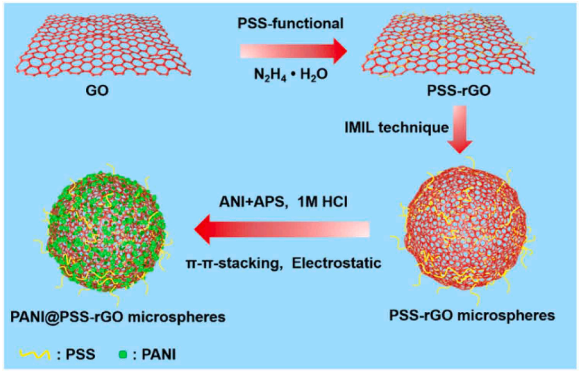
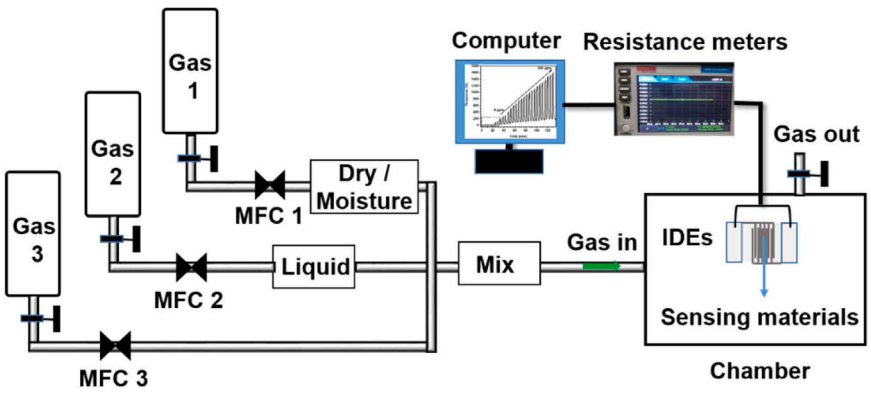


Fig. 1. Illustration of the preparation method of the sensing materials.



Scheme 1. Schematic diagram of the gas sensing measurements.

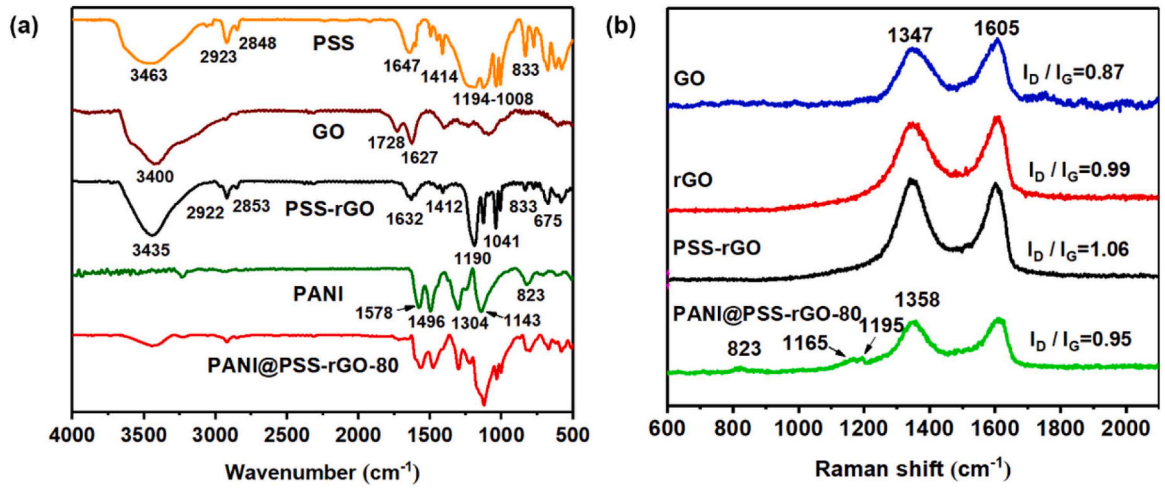


Fig. 2. (a) FTIR spectra of PSS, GO, PSS-rGO, PANI, and PANI@PSS-rGO-80; (b) Raman spectra of GO, rGO, PSS-rGO, and PANI@PSS-rGO-80.

the CH_2. The peaks at 675 cm^{-1} and 833 cm^{-1} corresponded to the stretching vibration modes of the C–S benzenoid ring and to the out-of-plane bending mode of the para-disubstituted benzene, respectively [36]. The characteristic carboxyl peaks at 1728 cm^{-1} and the hydroxyl at 3400 cm^{-1} of GO were attenuated in the PSS-rGO spectrum. We attributed the absorption peak at 1496 cm^{-1} to the C═C stretching of quinoid and the peak at 1578 cm^{-1} to the benzoid rings in the pure PANI spectrum, respectively. The peaks at 823 cm^{-1}, 1143 cm^{-1}, and 1304 cm^{-1} were attributed to the C–H out-of-plane bending vibration and the C–H in-plane bending vibration of the benzene ring in PANI, and the C–N stretching mode of the benzene unit, respectively [28,37]. The FTIR spectrum of PANI@PSS-rGO-80 revealed peaks associated with both PSS-rGO and PANI, demonstrating that the polymerization of PANI on the surface of the PSS-rGO microspheres was successful. Fig. 2b shows the Raman spectra of the GO, rGO, PSS-rGO, and PANI@PSS-rGO-80. The Raman spectra of rGO, GO, and PSS-rGO exhibited two main peaks at around 1605 cm^{-1} and 1347 cm^{-1}, which aligned with the graphene's G-band (tangential vibration of sp2 carbon atoms) and D-band (sp3 defects), respectively [38]. According to the Raman spectrum of PSS-rGO, the I_D/I_G intensity ratio (1.06) was higher than that of GO (0.87). The increased defects on the PSS-rGO were the results of the PSS functional modification of GO and the efficient removal of the oxygen-containing groups of GO, which occurred in the chemical reduction [39]. Interestingly, PSS-rGO showed an even higher I_D/I_G value than rGO (0.99), proving that the graphene structure was not disrupted during the supramolecular assembly process. The peaks at 1195 cm^{-1}, 1165 cm^{-1}, and 823 cm^{-1} aligned with the C–N stretching vibrations in polaronic units, the in-plane C–H bending vibrations of the benzoid ring, and the out-of-plane C—H bending of the quinoid ring for PANI@PSS-rGO-80, respectively. This result was

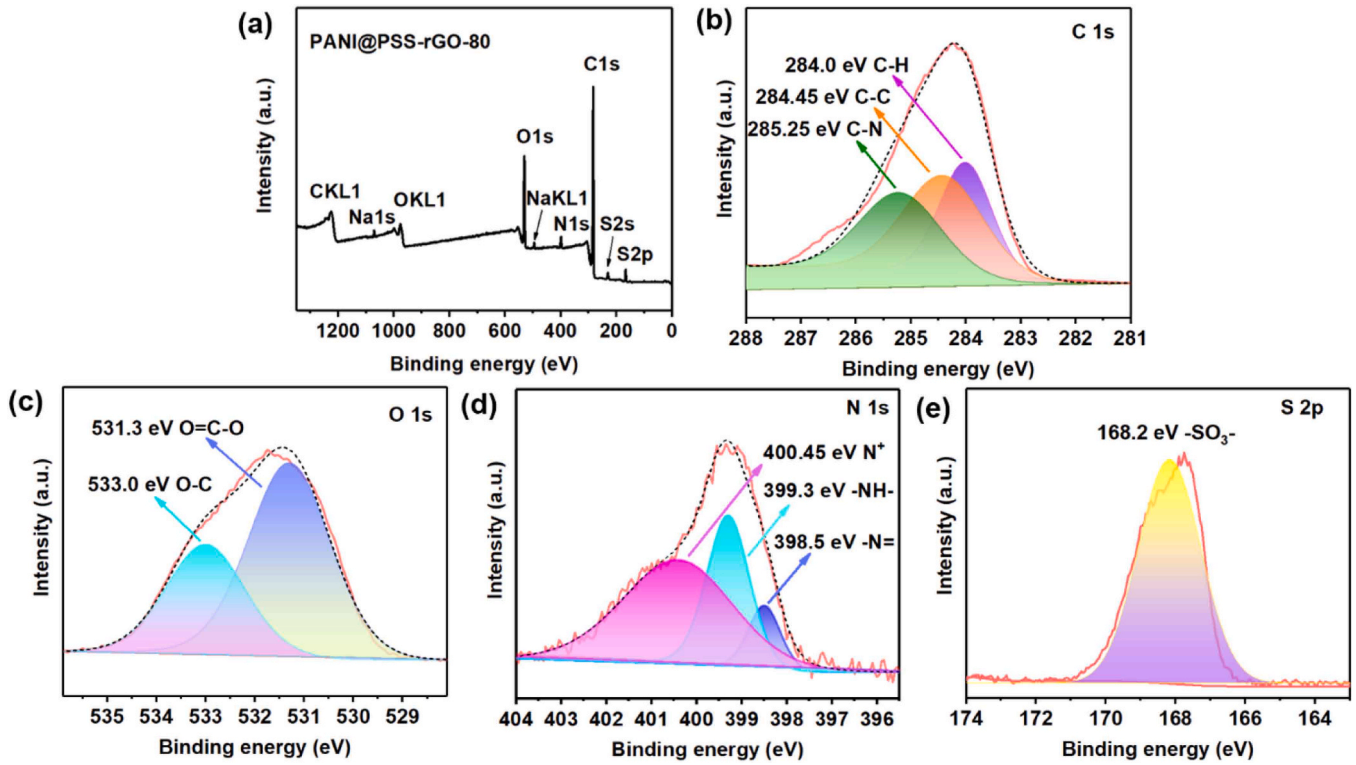


Fig. 3. XPS survey scan of (a) PANI@PSS-rGO-80 and narrow scan spectra of (b) C 1 s, (c) O 1 s, (d) N 1 s, and (e) S 2p.

consistent with the characteristic peaks of PANI [40]. We compared the G-band and D-band positions of the PANI@PSS-rGO-80 with PSS-rGO and found they upshifted by about 4 cm^{-1} and 11 cm^{-1}, respectively. This result revealed that, through the π–π and electrostatic interactions, PANI was successfully polymerized onto the hollow 3D PSS-rGO microspheres.

The elemental composition and protonation states of PANI@PSS-rGO-80 were measured using X-ray photoelectron spectroscopy (XPS). Fig. 3 shows the XPS wide-scan spectra and high-resolution spectra of C 1 s, O 1 s, N 1 s, and S 2p. The PANI@PSS-rGO-80 peaks at 167.75, 231.00, 284.25, 399.35, and 531.75 eV were assigned to S 2p, S 2 s, C 1 s, N 1 s, and O 1 s, respectively (Fig. 3a). As shown in Fig. 3b, the deconvoluted C 1 s spectrum exhibited three binding states with binding energies of 285.25 eV, 284.45 eV, and 284.0 eV, which aligned with the C−N, C−C, and C−H bonds, respectively [29]. According to Fig. 3c, the O 1 s spectrum was deconvoluted and two independent peaks appeared at 533.0 eV and 531.3 eV, which corresponded to O−C and O═C−O bonds, respectively. These results indicated a strong interaction between the PSS-rGO microspheres and PANI [41]. As shown in Fig. 3d, the N 1 s spectrum of PANI@PSS-rGO-80 was deconvoluted into three independent peaks at 400.45 eV (N^+, protonated amine), 399.3 eV (−NH−, benzenoid amine), and 398.5 eV (−N = , quinoid imine) [29,36,42], indicating the presence of protonated PANI. In addition, we determined the protonation level of PANI@PSS-rGO-80 using the ratio of the N^+ species (sum of $–NH^{\bullet+}$) to the N species (sum of –N = , –NH–, and $–NH^{\bullet+}$). The high protonation level of PANI@PSS-rGO-80 (with an N^+/N ratio of 0.69) is due to the sulfonate dopant keeping the PANI in its conductive salt form. According to the results of the N 1 s spectrum, we further confirmed the C-N absorption peaks at 1304 cm^{-1} and the C═N stretching vibration peaks at 1496 cm^{-1} in the FTIR analysis, as well as the C–N peak at 1195 cm^{-1} in the Raman spectra. Because of the enhanced π–π interaction between the PANI and the PSS-rGO microspheres, an improved doping level and a longer path for delocalized electrons can be achieved in the PANI [36]. A clear S 2p peak at 168.2 eV, which aligned with the $-SO_3-$ groups of PSS, was revealed in the XPS spectrum shown in Fig. 3e. The results of XPS analysis showed 77% carbon, 17% oxygen, 3.4% nitrogen, and 2.6% sulfur in the PANI@PSS-rGO-80 surface (Table S1).

We used FESEM and TEM to characterize the morphologies of the rGO, PSS-rGO nanosheets, pure PANI, PANI@PSS-rGO composites, and PSS-rGO microspheres. The pure PANI shows a relative fibrous structure while the rGO shows a stacking structure (Figs. S1a, b). Compared with the PSS-rGO nanosheets, the PSS-rGO microspheres have a hollow 3D spherical structure (Figs. S1c, d). The functionalization of PSS not only inhibits graphene restacking via π–π interactions with graphene, but also provides an electrostatic driving force that facilitates microsphere formation [24]. As shown in Fig. S2, compared with PANI@PSS-rGO-80, other PANI@PSS-rGO composites exhibit a similar microsphere structure but contain more chain-like structures and more collapsed microspheres. This phenomenon is attributed to the higher aniline proportion in other PANI@PSS-rGO composites. For PANI@PSS-rGO-90, the excess PSS-rGO microspheres were not supported by PANI and thus showed disintegrated structures. For comparison, the PANI/PSS-rGO-90, PANI/PSS-rGO-70, PANI/PSS-rGO-50, PANI/PSS-rGO-30, and PANI/PSS-rGO-10 were prepared by using PSS-rGO nanosheets in the polymerization process. As shown in Fig. S3, these samples exhibited extended nanosheet structure with PANI on their surfaces. The advantages of the stable hollow 3D microsphere structure of PANI@PSS-rGO-80 were reflected in the performance of the sensor.

Compared with the pure PSS-rGO microspheres (Fig. 4a, b), in the case of PANI@PSS-rGO-80 microspheres, the PANI was compactly grown and uniformly distributed on both sides of the PSS-rGO microsphere surfaces (Fig. 4c, d). This condition was favorable to increase the specific surface area. The hollow 3D PSS-rGO microspheres and PANI@PSS-rGO-80 microspheres have an average particle size of approximately 1 −3 μm (Figs. S4a, b). In addition, the uniformly

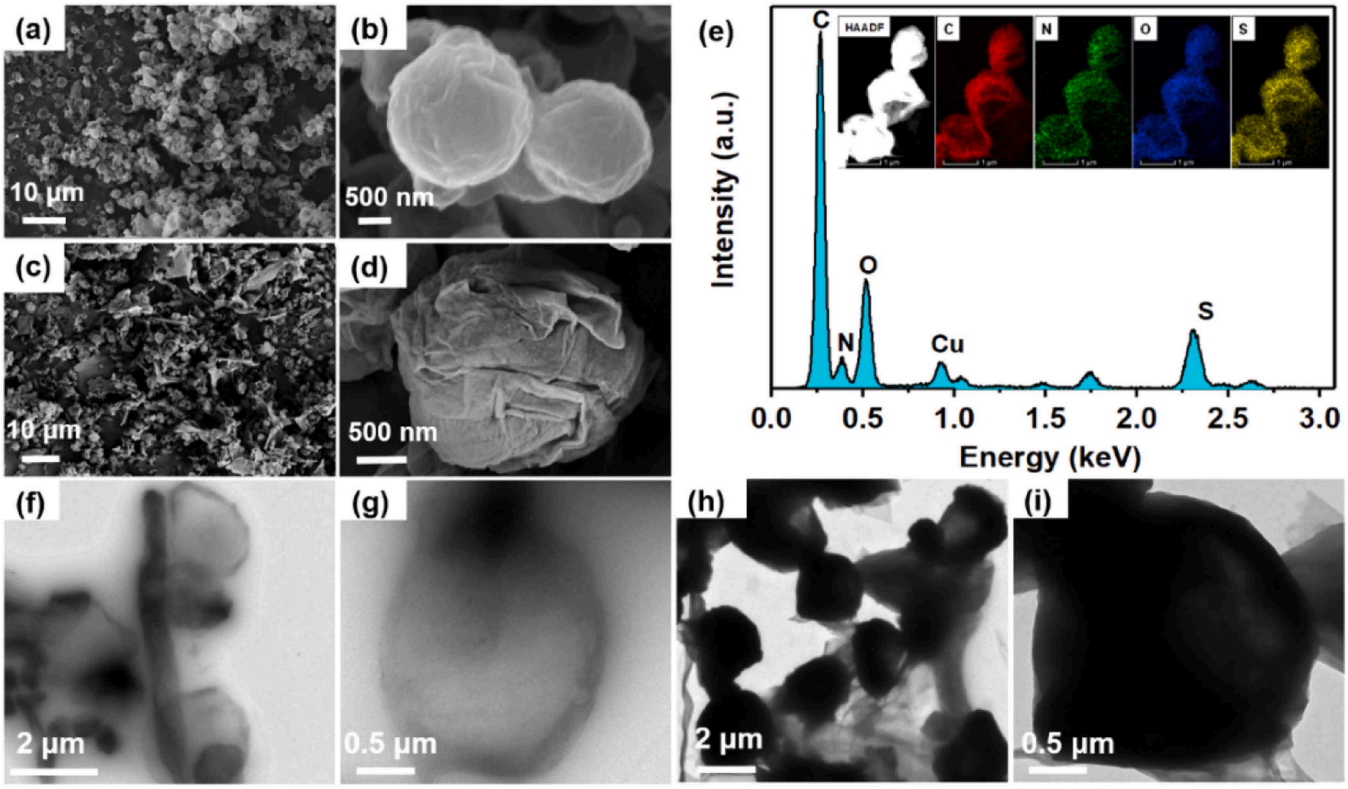


Fig. 4. SEM images of (a, b) PSS-rGO microspheres and (c, d) PANI@PSS-rGO-80 microspheres; EDS spectrum of (e) PANI@PSS-rGO-80 microspheres and C, N, O, S elemental mapping; TEM images of (f, g) PSS-rGO microspheres and (h, i) PANI@PSS-rGO-80 microspheres.

dispersed nano-sized PANI effectively improves the contact and adsorption rate of NH_3 on the sensing materials [22]. As a result, the NH_3 molecules could more easily diffuse across the surface of the sensing materials and thus could interact with the sensing materials more easily [43], which improved reversibility and activity. We also used TEM to assess the anchoring of PANI and its distribution across the PSS-rGO microsphere surface. EDS analysis and elemental mapping of C, O, N, and S in the PANI@PSS-rGO-80 microspheres showed that PANI was uniformly distributed across the surface of the PSS-rGO microspheres (Fig. 4e). The pure PSS-rGO microspheres exhibit a hollow 3D structure with a size of approximately 1.5 μm (Fig. 4f, g). After in situ polymerization, the resultants were found to be decorated with PANI, demonstrating the efficient bonding between the PSS-rGO and PANI (Fig. 4h, i). The PANI@PSS-rGO-80 microspheres exhibited a significantly greater thickness due to the polymerization of PANI onto the PSS-rGO surfaces. The BET results show that the PANI@PSS-rGO composite has a larger specific surface area (73.37 m^2/g) than pure PANI (30.43 m^2/g), which confirms that the hollow 3D structure is advantageous for NH_3 adsorption (Fig. S5). Even after the harsh chemical reaction, the PSS-rGO microspheres retained their original morphologies. Especially, when PANI@PSS-rGO composites were dispersed in water and dropped onto a substrate, their hollow 3D structure was maintained (Fig. S6), which has positive implications for applications. We confirmed that PANI@PSS-rGO microspheres could be synthesized successfully along our designed route according to the FTIR, Raman, XPS, and TEM results.

3.2. NH_3-sensing performance

The sensing performances of the sensors toward NH_3 gas were investigated. First, we found that as the polymerization time increases, the response performance gradually decreases. Considering the degree of polymerization, the optimal polymerization time should be 3 h (Fig. S7). Fig. 5a shows the dynamic response of PANI@PSS-rGO-10, PANI@PSS-rGO-20, PANI@PSS-rGO-33, PANI@PSS-rGO-50, PANI@PSS-rGO-66, PANI@PSS-rGO-80, and PANI@PSS-rGO-90, in which the response values were 46, 160, 241, 335, 465, 643, and 961%, respectively (Fig. S8a). Although the response of PANI@PSS-rGO-80 was lower than that of PANI@PSS-rGO-90, its response and recovery times (9 s and 120 s) were more desirable (Fig. S8b). Moreover, the response value of PANI@PSS-rGO-90 had a problem of instability resulting from the incomplete polymerization caused by the low reactant concentration of aniline monomer. Considering the response values and response/recovery times in Fig. S8, the PANI@PSS-rGO-80 sensor exhibited an optimal performance compared to the other sensors, indicating that the hollow 3D PANI@PSS-rGO-80 microsphere construction is promising for gas sensing applications. We examined the response values of PANI/PSS-rGO nanosheets and PANI@PSS-rGO microspheres to highlight the hollow 3D microsphere advantages. As shown in Fig. S9, the microspheres exhibited an optimal response value compared to the nanosheets. The superior properties of PANI@PSS-rGO microspheres are ascribed to the introduction of PSS-rGO microspheres enabling PANI to polymerize onto PSS-rGO [29]. The decorated PANI can increase the adsorption sites of PANI@PSS-rGO microspheres, which increases the overall interaction between sensitive materials and NH_3 gas molecules

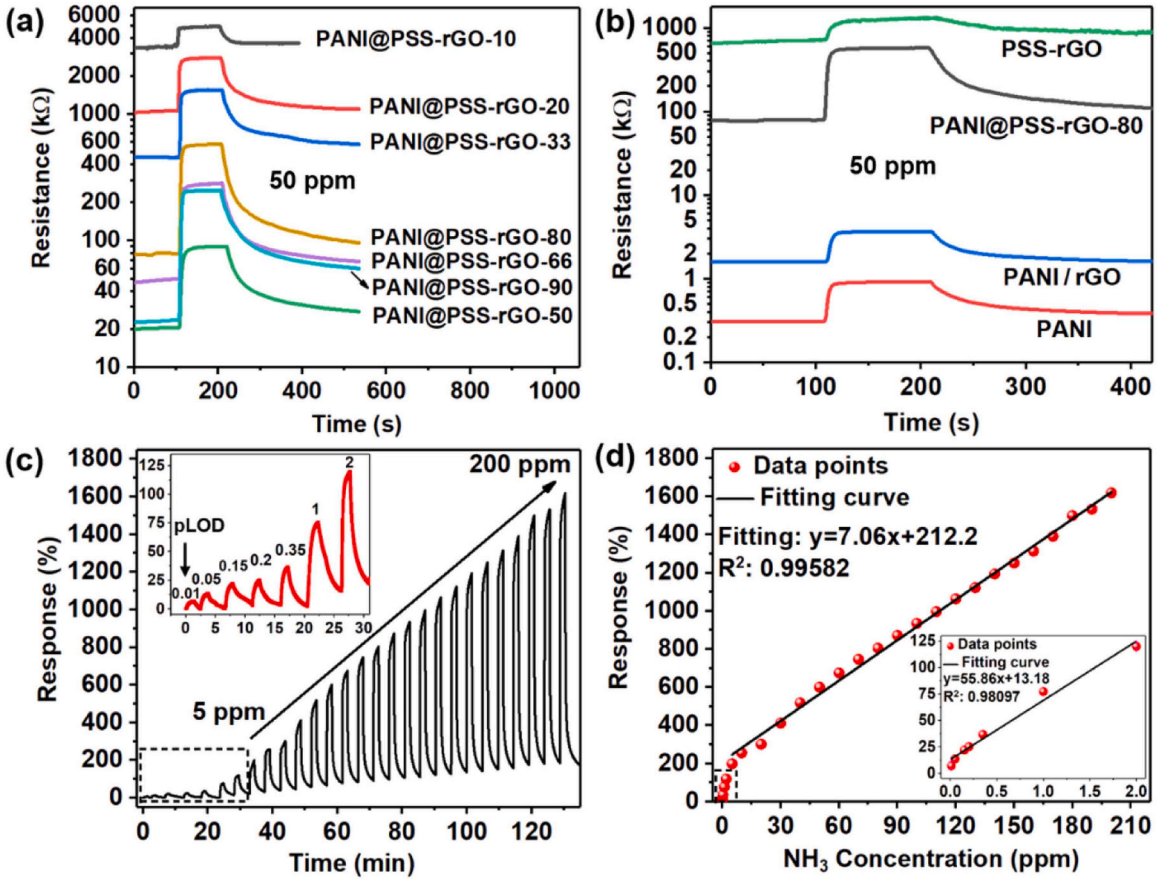


Fig. 5. Dynamic response of (a) PANI@PSS-rGO composites with various addition of PSS-rGO microspheres to 50 ppm NH_3; Response curve of (b) PSS-rGO microspheres, PANI / rGO composites, pristine PANI, and PANI@PSS-rGO-80-based sensors toward 50 ppm NH_3; Successive response curves of (c) the PANI@PSS-rGO-80-based sensor exposed to different NH_3 concentrations in the range of 0.01–200 ppm (including low-concentration analysis and pLOD shown in the inset); and (d) response value demonstrated in the corresponding linear fit.

[44].

We compared the sensing properties of the PANI@PSS-rGO-80 microspheres to NH_3 with those of PANI, PANI-rGO, and PSS-rGO microsphere sensors (Fig. 5b). According to the results shown in Fig. S10, after exposure to 50 ppm of NH_3, the PANI@PSS-rGO-80-based sensor had a relatively higher response value than the other sensors. The high response could be attributed to the good water dispersibility provided by PSS and to the synergistic effects of PANI and the PSS-rGO microspheres (Fig. S11). We investigated the response of the PANI@PSS-rGO-80-based sensor by exposing it to different concentrations of NH_3 (0.01, 0.05, 0.15, 0.2, 0.35, 1, 2, 5, 10, 20, 30, 40, 50, 60, 70, 80, 90, 100, 110, 120, 130, 140, 150, 160, 170, 180, 190, 200 ppm) at room temperature (Fig. 5c). The response of the sensor decreased as the NH_3 concentration decreased. The sensor had a response value of 7% toward 10 ppb NH_3. The Fig. 5c inset highlights the response in the 10 ppb to 2 ppm range of the PANI@PSS-rGO-80-based sensor. The linearly fitted plot is illustrated in Fig. 5d to highlight the relationship between concentrations of NH_3 (0.01–200 ppm) and the response value of PANI@PSS-rGO-80. The linear fitting equations are denoted as $Y\ (\%) = 7.06\ X + 212.20$ for the specific concentration range of 0.01–2 ppm, and $Y\ (\%) = 55.86\ X + 13.18$ for the specific concentration range of 5–200 ppm. The sensitivity (S) of the sensor is determined by the slope of the linear regression line fitted to the response-concentration data points. Such a high sensitivity (7.06% / ppm at high concentration and 55.86% / ppm at low concentration) can be attributed to the numerous unsaturated adsorption sites in the PANI@PSS-rGO-80 microsphere surfaces. The higher sensitivity at low concentrations is attributed to the nearly bare surface adsorption sites [45]. Importantly, the sensor response has an excellent linear relationship with NH_3 concentrations with a regression coefficient (R^2) of 0.99582 (5–200 ppm) and 0.98097 (0.01–2 ppm). Table 1 provides a summary of the high response of the PANI@PSS-rGO-80-based sensor and reveals that this sensor was competitive with existing NH_3 sensors. The low pLOD of 10 ppb renders the PANI@PSS-rGO-80-based sensor promising potential for commercial applications.

In addition, a key factor in the practical application of gas sensors is repeatability. Fig. 6a shows five response−recovery cycles of a single PANI@PSS-rGO-80-based sensor response toward 50 ppm NH_3. The maximum relative error of this sensor's response during the repeated cycling test is 9.07%. The response values for each NH_3 sensing cycle were well maintained and closely matched the fitting curve shown in Fig. 5d. As shown in Fig. S12, three repeated tests were conducted on each of the two independently fabricated sensors separately, and the standard deviations for Sensor 1 and Sensor 2 (calculated from their own respective three repeated tests) were determined to be 9.43% and 22.6%, respectively. The two independently fabricated sensors show consistent response toward 50 ppm NH_3 with a mean response value difference below 50% (drift less than 10%), demonstrating good device-to-device reproducibility. These results showed that it had good stability and thus it is a promising candidate for practical applications. After exposure to 500 ppm of various gas species (e.g., acetic acid, ethanol, acetone, formaldehyde, and methanol), PANI@PSS-rGO-80-based sensor exhibited high selectivity for 50 ppm NH_3 (Fig. 6b). Due to the excellent adsorption capacity of the PANI@PSS-rGO-80-based sensor for NH_3, its response to 50 ppm of NH_3 (643%) was higher than that of the other gases [55]. At the concentration of 500 ppm, we measured the response values of formaldehyde, acetic acid, ethanol, acetone, and methanol to be 9%, 4.6%, 1.58%, 0.56%, and 0.51%, respectively, which revealed the high selectivity of PANI@PSS-rGO-80 to NH_3. In addition, we investigated the long-term stability of the PANI@PSS-rGO-80-based sensor by exposing it to 50 ppm of NH_3 for 75 days (Fig. 6c). During the first month, as unstable adsorption sites disappeared, the PANI@PSS-rGO-80-based sensor's response gradually declined [26]. Even after 75 days, the response value remained above 80%, which demonstrated the PANI@PSS-rGO-80-based sensor's good stability.

Fig. 6d shows the real-time resistance variation of the PANI@PSS-rGO-80-based sensor when sequentially exposed to 20 ppm NH_3 at relative humidity ranging from 20% to 80%, which directly reveals the dynamic sensing and recovery behavior under different humidity environments. This tendency can be explained by the combined effects of protonation and swelling effects [56,57]. Water molecules adsorbed on the sensor surface were converted into hydroxyl ions (OH^-) and protons (H^+), which improved the doping degree and decreased the baseline resistance of the PANI@PSS-rGO-80. The swelling effects demonstrated that the PANI chain segments were disordered or distorted because of water molecule absorption, which blocked charge carrier movement and increased the baseline resistance. As shown in Fig. 6e, the response of the PANI@PSS-rGO-80 sensor gradually increased as the relative humidity increased from 20% to 60%. However, a slight decrease in response occurred with further increases in relative humidity, demonstrating a RH-dependent response behavior. Between 20% RH and 60% RH, the protonation effect dominated and improved the response of the PANI@PSS-rGO-80-based sensor to NH_3. However, the response of the PANI@PSS-rGO-80-based sensor toward NH_3 decreased in overwet conditions (>60% RH). This result can be ascribed to the competition adsorption between NH_3 and H_2O, where H_2O molecules occupied active sites and weakened the sensing response. Therefore, it was necessary to adopt humidity compensation to mitigate the negative influence of water on sensing characteristics [25]. To support quantitative humidity compensation, Fig. 6f presents the baseline resistance variation of the PANI@PSS-rGO-80-based sensor in the absence of NH_3 under 10%−70% RH. As relative humidity increased from 10% to 70%, the resistance decreased from 308 kΩ to 136 kΩ with a relative change rate of 55.84%. The hydrophilicity of poly (sodium p-styrenesulfonate) is responsible for the remarkable resistance variation observed [36,58].

Table 1
NH_3-sensing performances for typical conducting polymer-based sensors at room temperature.

Materials and structure	Structure/ Morphology	NH_3 (ppm)	Response (%)	T_{res} / T_{rec} (s)	D_R (ppm)	LOD (ppm)
RGO-PANI [46]	Hybrid	50	59.2	800/200	–	1
PPy/rGO [47]	Nanosheet	1	6.1	60/300	1 –4	< 1
PEDOT/RGO [48]	Porous	5	2.1	< 100/< 180	0.2 –10	–
S, N: GQDs/PANI [49]	Film	100	42.3	115/44	1 –1000	1
PANI/rGO/SnO_2[50]	Hybrid	100	45	40/45	–	–
MNPA-100 [11]	Hybrid	100	185.44	231.2/165.4	1.77 –100	1.77
PANI-PDA-BF [17]	Fiber	100	521	> 180/> 300	10 –120	10
NiNPs@3D(N)GFs/PANI [51]	3D frameworks	100	89.5	95/32	1 –1000	1
PANI@rGO@SiO_2[33]	3D microsphere	100	111	1.09/1.81	0.5 –100	0.5
PANI@3D C-FW CPs [52]	3D frameworks	10	~20	15/–	0.1 –100	0.1
Ppy-C@PANI [53]	3D frameworks	100	224.53	59.5/25.6	2–100	0.47
PANI/LIG [54]	3D porous	60	68	53/167	0.5–150	0.5
PANI/CuO@3D-NGF [28]	3D frameworks	100	930	30/57	–	0.05
This work	**3D microsphere**	**50**	**643**	**9/120**	**0.01 –200**	**0.01** (pLOD)

Note: T_{res} = Response time; T_{rec} = recovery time; D_R = studied detection range; pLOD = practical limit of detection.

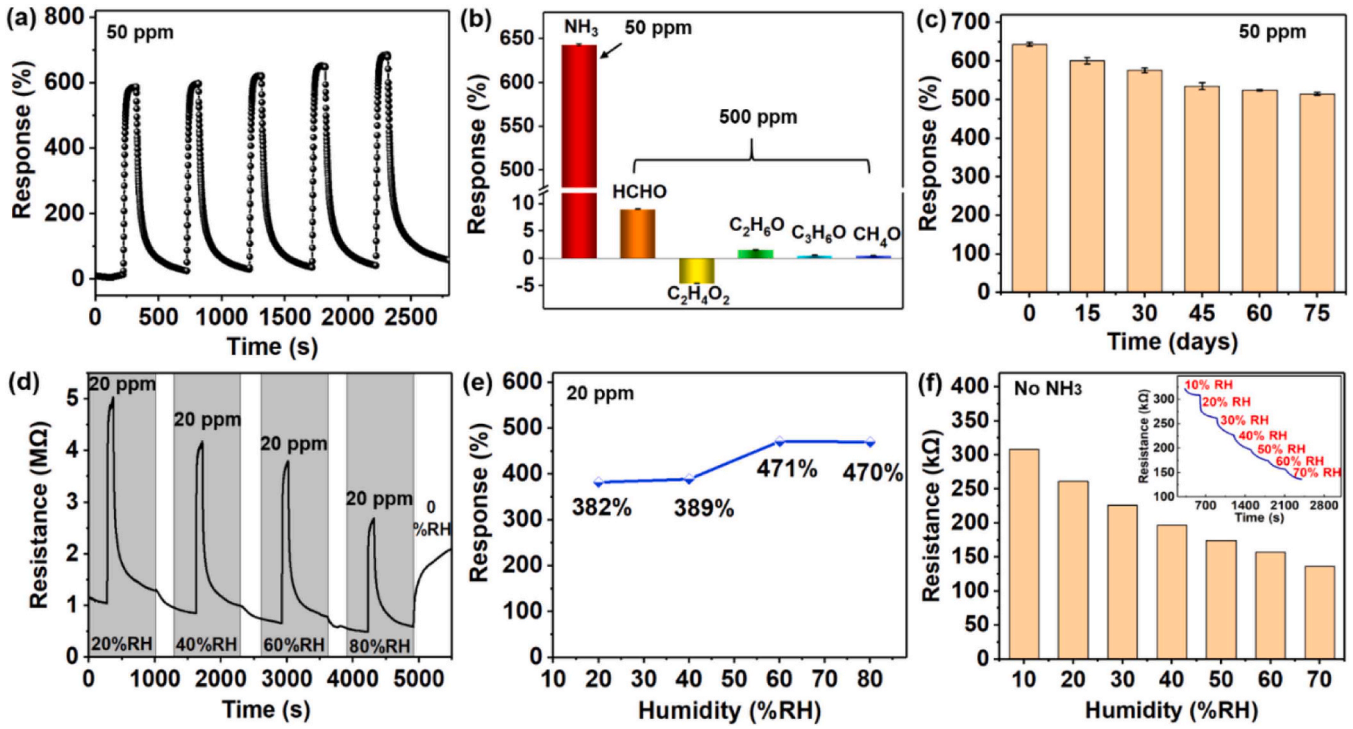


Fig. 6. Repeated response of (a) a single PANI@PSS-rGO-80-based sensor successive exposure (5 cycles) to 50 ppm NH_3; Selectivity of (b) PANI@PSS-rGO-80 to different test gases at concentrations of 500 ppm as well as 50 ppm NH_3, the sensors were tested 3 times for obtaining the responses and error bars; Long-term stability of (c) PANI@PSS-rGO-80-based sensor exposed toward 50 ppm NH_3; Response curve of (d) the PANI@PSS-rGO-80-based sensor; and (e) corresponding response value of 20 ppm NH_3 at room temperature, ranging from 20% to 80% RH; (f) PANI@PSS-rGO-80 sensor's resistance variation in the absence of NH_3 at relative humidity ranging from 10% to 70% RH, where the upper-right inset presents the sensor resistance as a function of humidity.

After humidity compensation, the sensor is capable of meeting the requirements for practical NH_3 detection.

3.3. Sensing mechanism

The PANI-based sensing materials exhibit p-type semiconductor behavior toward NH_3. Typically, the protonated PANI (Emeraldine Salt, ES) reacts with NH_3 to form NH_4^+ and deprotonated PANI (Emeraldine Base, EB), increasing the resistance of the PANI-based sensing materials [59,60]. Once NH_3 is removed, the resistance recovers to its original state. This reversible sensing process can be summarized by formula (1). Formula (2) shows the NH_3 sensing mechanism of the PANI/PSS-rGO

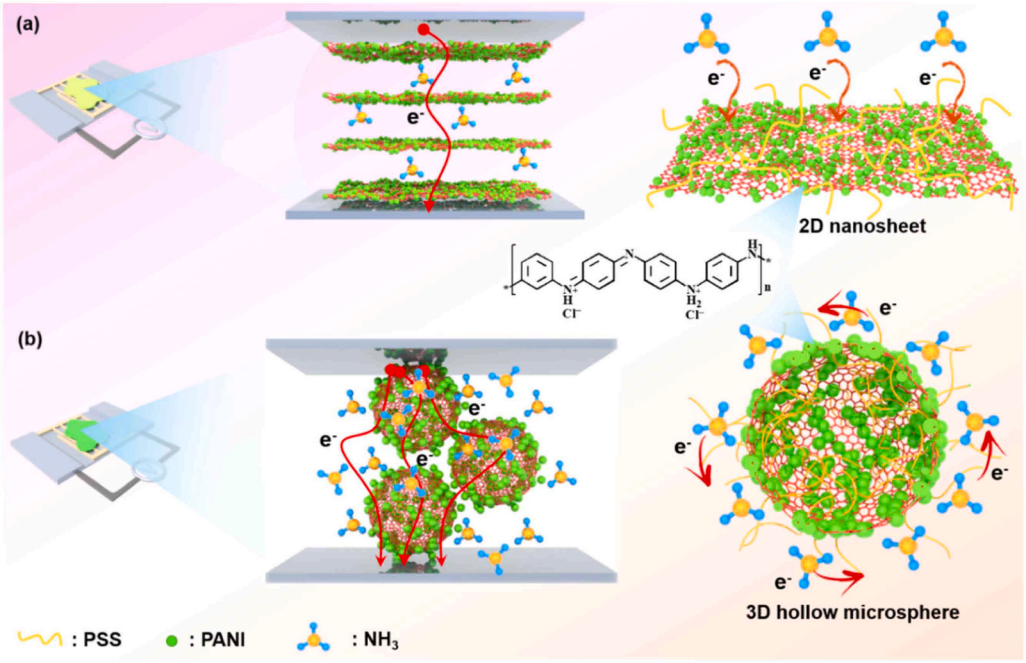


Fig. 7. Illustration of the NH_3 sensing mechanism in (a) 2D PANI/PSS-rGO nanosheet and (b) hollow 3D PANI@PSS-rGO-80 microsphere.

nanosheet (Fig. 7a). PSS-rGO had high conductivity, which enabled the electrical charges to transfer throughout the sensing process [58].

$NH_3 + HN^+$-PANI (ES) ⇋ N-PANI (EB)+ NH_4^+ formula (1)

$NH_3 + HN^+$-PANI/PSS-rGO (ES) ⇋ N-PANI/PSS-rGO (EB)+ NH_4^+ formula (2)

$NH_3 + HN^+$-PANI@PSS-rGO (ES) ⇋ N-PANI@PSS-rGO (EB)+ NH_4^+ formula (3)

The sensing mechanism of PANI@PSS-rGO-80 microspheres for NH_3 can be proposed in formula (3) and Fig. 7b. First, TEM and SEM images revealed that the PSS-rGO microspheres had a hollow 3D spherical structure (Fig. 4). The BET-measured large specific surface area (73.37 m^2/g) of PANI@PSS-rGO provides increased specific surface area, enhancing NH_3 adsorption, protonation-deprotonation efficiency, thus amplifying the sensor response. Second, the PANI is firmly decorated onto the PSS-rGO microspheres to provide numerous adsorption sites for NH_3 adsorption. The XPS results in Fig. 3d confirm that the PANI@PSS-rGO-80 microspheres have a high protonation level (0.69). PSS not only acts as a sulfonate dopant to maintain PANI in its conductive salt form with a high protonation level but also inhibits graphene restacking via π–π interactions with graphene and PANI, thereby optimizing the composite's gas sensing performance. Third, charge transfer between PANI and PSS-rGO can occur through delocalized electrons during the sensing process. Although PSS-rGO exhibits lower conductivity than PANI (Fig. 5b), a higher proportion of PSS-rGO in the PANI@PSS-rGO composite enables the formation of conductive networks (Fig. S2), leading to enhanced conductivity (Fig. 5a). Consequently, the conductive networks functioning as fast charge transfer channels can be formed within the PANI@PSS-rGO-80. When the PANI@PSS-rGO-80-based sensor is exposed to NH_3, NH_3 is easily adsorbed onto the PANI to provide charge for rapid transfer to the PSS-rGO sensing channel and finally to the electrodes. Fourth, the sensing results demonstrated that the response and recovery speed and the response value of the sensor to NH_3 improved in the hollow 3D PANI@PSS-rGO-80 microspheres (Fig. 5b and Fig. S8). We attributed the improvement in NH_3 sensing performance to the synergistic effect of the sufficient adsorption sites of PANI, the microsphere's large specific surface area, and the fast multichannel charge transfer of the graphene-based sensing network.

4. Conclusion

In summary, PSS-rGO microspheres were prepared using the IMIL technique. We synthesized PANI@PSS-rGO composites using an in situ chemical oxidation polymerization. The π–π interactions among PSS, graphene, and PANI are responsible for the compact packing of the PANI on the surfaces of the PSS-rGO microspheres and its high protonation states. The PSS-rGO microspheres had a hollow 3D morphology with an average size of 1–3 μm, which created a large specific surface area with sufficient gas adsorption sites. The PANI@PSS-rGO-80 sensor demonstrated high response (643%) with short response and recovery times (9 s and 120 s) to 50 ppm of NH_3. It also demonstrated good repeatability, selectivity, and long-term stability at room temperature. The obtained sensor exhibited detectable sensitivity to 10 ppb of NH_3 with a response value of 7%, and demonstrated a linear response over a range of NH_3 concentrations. We attribute the exceptional NH_3 sensing performance of the PANI@PSS-rGO-80 sensor to its hollow 3D microsphere structure with fast multichannel charge transfer and large specific surface area. Because of the influence of protonation and swelling effects, the sensing response increased in the range of 20–60% RH; however, due to competitive adsorption between NH_3 and water, it decreased slightly at 80% RH. The novel protonated PANI decorated PSS-rGO microspheres are a promising candidate for both environmental and disease diagnosis applications with stable and trace monitoring properties.

CRediT authorship contribution statement

Min Zeng: Project administration, Formal analysis. **Zhenting Zhao:** Visualization, Software. **Yao Wang:** Writing – review & editing, Methodology, Funding acquisition, Conceptualization. **Hongping Liang:** Writing – original draft, Methodology, Investigation, Funding acquisition, Conceptualization. **Guofu Zhou:** Funding acquisition. **Zhuo Chen:** Validation, Methodology, Data curation. **Zilun Tang:** Writing – review & editing, Investigation, Formal analysis. **French Patrick James:** Visualization. **Fei Wang:** Writing – review & editing, Resources. **Hao Li:** Validation. **Quan Wang:** Software. **Weiping Gong:** Writing – review & editing, Supervision, Funding acquisition.

Declaration of Competing Interest

The authors declare that they have no known competing financial interests or personal relationships that could have appeared to influence the work reported in this paper.

Acknowledgments

This work was supported by the Basic and Applied Basic Research Foundation of Guangdong Province (2025A1515012116, 2023A1515110940, 2023A1515140074), the Huizhou Introduces and Cultivates Scientific and Technological Talents (Team) Project (2023EQ050033), the Huizhou University Independent Innovation Capability Enhancement Plan Project (HZU202513), Guangdong Provincial Key Laboratory of Optical Information Materials and Technology (2023B1212060065), the 111 Project.

Data availability

Data will be made available on request.

Raw sensing data and calibration datasets (Raw sensing data and calibration datasets)

References

[1] M.P. Diana, W.S. Roekmijati, W.U. Suyud, Hadiyanto, Maryono, B. Warsito, Why it is often underestimated: historical study of ammonia gas exposure impacts towards human health, E3s Web Conf. 73 (2018) 06003, https://doi.org/10.1051/e3sconf/20187306003.

[2] L. Du, D. Feng, X. Xing, C. Wang, Y. Gao, S. Sun, G. Meng, D. Yang, Nanocomposite-decorated filter paper as a twistable and water-tolerant sensor for selective detection of 5 ppb-60 v/v% ammonia, ACS Sens 7 (2022) 874–883, https://doi.org/10.1021/acssensors.1c02681.

[3] J.W. Yoon, J.H. Lee, Toward breath analysis on a chip for disease diagnosis using semiconductor-based chemiresistors: recent progress and future perspectives, Lab. Chip 17 (2017) 3537–3557, https://doi.org/10.1039/C7LC00810D.

[4] X. Duan, Z. Duan, Y. Zhang, B. Liu, X. Li, Q. Zhao, Z. Yuan, Y. Jiang, H. Tai, Enhanced NH_3 sensing performance of polyaniline via a facile morphology modification strategy, Sens. Actuators B Chem. 369 (2022) 132302, https://doi.org/10.1016/j.snb.2022.132302.

[5] X. Xing, L. Du, D. Feng, C. Wang, Y. Tian, Z. Li, H. Liu, D. Yang, Twistable and tailorable V_2O_5/PANI/GO nanocomposites textile for wearable ammonia sensing, Sens. Actuators B Chem. 351 (2022) 130944, https://doi.org/10.1016/j.snb.2021.130944.

[6] Z. Tian, P. Song, Z. Yang, Q. Wang, Reduced graphene oxide-porous In_2O_3 nanocubes hybrid nanocomposites for room-temperature NH_3 sensing, Chin. Chem. Lett. 31 (2020) 2067–2070, https://doi.org/10.1016/j.cclet.2020.01.025.

[7] S.H. Lee, W. Eom, H. Shin, R.B. Ambade, J.H. Bang, H.W. Kim, T.H. Han, Room-temperature, highly durable Ti_3C_2Tx MXene/graphene hybrid fibers for NH_3 gas sensing, ACS Appl. Mater. Interfaces 12 (2020) 10434–10442, https://doi.org/10.1021/acsami.9b21765.

[8] J. Wu, Y. Wei, H. Ding, Z. Wu, X. Yang, Z. Li, W. Huang, X. Xie, K. Tao, X. Wang, Green synthesis of 3D chemically functionalized graphene hydrogel for high-performance NH_3 and NO_2 detection at room temperature, ACS Appl. Mater. Interfaces 12 (2020) 20623–20632, https://doi.org/10.1021/acsami.0c00578.

[9] Y. Li, Y. Li, Y. Shi, J. Gao, J. Lu, C. Wang, J. Chang, Z. Wang, Y. Yang, B. Yang, L. Feng, Q. Fu, X. Bao, Z.-S. Wu, Single cobalt atoms with unconventional dynamic coordination mechanism for selective ammonia sensor, Natl. Sci. Rev. 12 (2025) 31, https://doi.org/10.1093/nsr/nwaf031.

[10] T. Zhang, H. Qi, Z. Liao, Y.D. Horev, L.A. Panes-Ruiz, P.S. Petkov, Z. Zhang, R. Shivhare, P. Zhang, K. Liu, V. Bezugly, S. Liu, Z. Zheng, S. Mannsfeld, T. Heine, G. Cuniberti, H. Haick, E. Zschech, U. Kaiser, R. Dong, X. Feng, Engineering crystalline quasi-two-dimensional polyaniline thin film with enhanced electrical and chemiresistive sensing performances, Nat. Commun. 10 (2019) 1–9, https://doi.org/10.1038/s41467-019-11921-3.
[11] L. Lu, C. Zhang, Y. Zou, F. Xu, L. Sun, C. Xiang, Room-temperature humidity-resistant highly sensitive ammonia sensor based on a porous MXene/$Na_2Ti_3O_7$ @polyaniline composite, Sens. Actuators B Chem. 405 (2024) 135323, https://doi.org/10.1016/j.snb.2024.135323.
[12] Z. Wang, L. Ni, X. Zhang, L. Feng, A novel flexible substrate-free NH_3 sensing membrane based on PANI covered rGO functionalized fiber, Sens. Actuators B Chem. 380 (2023) 133307, https://doi.org/10.1016/j.snb.2023.133307.
[13] X. Wang, Y. Fu, F. Li, Z. Sun, C. Zhu, G. Zhao, X. Xu, Multi-heterostructure and surface free radicals induced enhanced ammonia gas sensing performance of polyaniline/tin phosphide/nitrogen-doped reduced graphene oxide at room temperature, J. Colloid Interface Sci. 698 (2025) 138122, https://doi.org/10.1016/j.jcis.2025.138122.
[14] S.L. Amith, K. Gurunathan, Active sites tailored rGO-PPy nanosheets with high crystalline tetragonal SnO_2 nanocrystals for ammonia e-sensitization at room temperature, J. Alloy. Compd. 960 (2023) 170819, https://doi.org/10.1016/j.jallcom.2023.170819.
[15] P.-G. Su, M.-S. Tsai, C.-J. Lu, Fabrication of noble metal (Au, Ag, Pt)/polythiophene/reduced graphene oxide ternary nanocomposites for NH_3 gas sensing at room temperature, Anal. Methods 14 (2022) 4113–4121, https://doi.org/10.1039/d2ay01317g.
[16] X. Liu, W. Zheng, R. Kumar, M. Kumar, J. Zhang, Conducting polymer-based nanostructures for gas sensors, Coord. Chem. Rev. 462 (2022) 214517, https://doi.org/10.1016/j.ccr.2022.214517.
[17] P. Tang, Y. Liu, Y. Tang, H. Zhang, Q. Wang, Mussel-inspired washable, fatigue-resistant, and environmental-friendly smart textile for monitoring NH_3, Sens. Actuators B Chem. 430 (2025) 137404, https://doi.org/10.1016/j.snb.2025.137404.
[18] C. Zhu, X. Dong, C. Guo, L. Huo, S. Gao, Z. Zheng, X. Cheng, Y. Xu, Template-free synthesis of a wafer-sized polyaniline nanoscale film with high electrical conductivity for trace ammonia gas sensing, J. Mater. Chem. A 10 (2022) 12150–12156, https://doi.org/10.1039/D2TA01825J.
[19] W. Yuan, G. Shi, Graphene-based gas sensors, J. Mater. Chem. A 1 (2013) 10078–10091, https://doi.org/10.1039/c3ta11774j.
[20] H. Liang, H. Hu, J. Wang, H. Li, N.F. d Rooij, G. Zhou, Y. Wang, Graphene-based room temperature gas sensing materials, Curr. Chin. Sci. 1 (2020) 98–114, https://doi.org/10.2174/2665997201999200729164157.
[21] L. Dong, Z. Chen, X. Zhao, J. Ma, S. Lin, M. Li, Y. Bao, L. Chu, K. Leng, H. Lu, K. P. Loh, A non-dispersion strategy for large-scale production of ultra-high concentration graphene slurries in water, Nat. Commun. 9 (2018) 76, https://doi.org/10.1038/s41467-017-02580-3.
[22] Z. Wu, X. Chen, S. Zhu, Z. Zhou, Y. Yao, W. Quan, B. Liu, Enhanced sensitivity of ammonia sensor using graphene/polyaniline nanocomposite, Sens. Actuators B Chem. 178 (2013) 485–493, https://doi.org/10.1016/j.snb.2013.01.014.
[23] X. Huang, X. Qi, F. Boey, H. Zhang, Graphene-based composites, Chem. Soc. Rev. 41 (2012) 666–686, https://doi.org/10.1039/C1CS15078B.
[24] Z. Chen, J. Wang, X. Liu, Y. Wang, J. Shen, J. Li, X. Liu, X. Li, W. Pei, Y. Guo, G. Shi, H. Li, A.M.U. Siddiqui, N.F. de Rooij, L. Jiang, G. Zhou, Crafting hollow spheres via bulk ice melting with ppb-level gas sensing performance, J. Am. Chem. Soc. 147 (2025) 3478–3487, https://doi.org/10.1021/jacs.4c14808.
[25] J. Wei, B. Liang, Q. Cao, C. Mo, Y. Zheng, X. Ye, Vertically aligned PANI nanorod arrays grown on graphene oxide nanosheets for a high-performance NH_3 gas sensor, RSC Adv. 7 (2017) 33510–33520, https://doi.org/10.1039/c7ra04636g.
[26] S. Li, T. Wang, Z. Yang, J. He, J. Wang, L. Zhao, H. Lu, T. Tian, F. Liu, P. Sun, X. Yan, G. Lu, Room temperature high performance NH_3 sensor based on GO-rambutan-like polyaniline hollow nanosphere hybrid assembled to flexible PET substrate, Sens. Actuators B Chem. 273 (2018) 726–734, https://doi.org/10.1016/j.snb.2018.06.072.
[27] K. Stephen Dongmin, S.G. Jeffrey, Charge-transport model for conducting polymers, Nat. Mater. 16 (2017) 252–257, https://doi.org/10.1038/nmat4784.
[28] F.A. Tabar, A. Nikfarjam, N. Tavakoli, J.N. Gavgani, M. Mahyari, S.G. Hosseini, Chemical-resistant ammonia sensor based on polyaniline/CuO nanoparticles supported on three-dimensional nitrogen-doped graphene-based framework nanocomposites, Microchim. Acta 187 (2020) 293, https://doi.org/10.1007/s00604-020-04282-y.
[29] H. Wang, S. Nie, H. Li, R. Ali, J. Fu, H. Xiong, J. Li, Z. Wu, W.M. Lau, N. Mahmood, R. Jia, Y. Liu, X. Jian, 3D hollow quasi-graphite capsules/polyaniline hybrid with a high performance for room-temperature ammonia gas sensors, ACS Sens 4 (2019) 2343–2350, https://doi.org/10.1021/acssensors.9b00882.
[30] G. Wang, J. Jin, Z. Li, Y. Dong, J. Yu, Z. Qiao, N. Luo, Novel multifunctional triboelectric nanogenerator based on PSS-PANI/copper foam composite for self-powered ammonia sensing and food spoilage detection, Chem. Eng. J. 505 (2025) 159614, https://doi.org/10.1016/j.cej.2025.159614.
[31] I.Y. Choi, J. Lee, H. Ahn, J. Lee, H.C. Choi, M.J. Park, High-conductivity two-dimensional polyaniline nanosheets developed on ice surfaces, Angew. Chem. Int. Ed. 54 (2015) 10497–10501, https://doi.org/10.1002/ange.201503332.
[32] X. Su, L. Gao, F. Zhou, G. Duan, A substrate-independent fabrication of hollow sphere arrays via template-assisted hydrothermal approach and their application in gas sensing, Sens. Actuators B Chem. 251 (2017) 74–85, https://doi.org/10.1016/j.snb.2017.05.024.
[33] J. Li, S. Dong, Y. Duan, X. Fu, G. Li, Y. Huang, Polyaniline composited with rGO wrapped-SiO_2 microsphere ammonia sensor with fast response/recovery and high sensitivity for pig healthy breeding, Sens. Actuators B Chem. 398 (2024) 134784, https://doi.org/10.1016/j.snb.2023.134784.
[34] L. Sun, Y. Shi, L. Chu, X. Xu, J. Liu, Preparation of polyaniline coated polystyrene-poly(styrene-co-sodium 4-styrenesulfonate) microparticles and the further fabrication of hollow polyaniline microspheres, J. Appl. Polym. Sci. 126 (2012) 870–876, https://doi.org/10.1002/app.36322.
[35] H. Liang, L. Guo, N. Cao, H. Hu, H. Li, N.F. Rooij, A. Umar, H. Algarni, Y. Wang, G. Zhou, Practical room temperature formaldehyde sensing based on a combination of visible-light activation and dipole modification, J. Mater. Chem. A 9 (2021) 23955–23967, https://doi.org/10.1039/D1TA06346D.
[36] S. Cho, J.S. Lee, J. Jun, S.G. Kim, J. Jang, Fabrication of water-dispersible and highly conductive PSS-doped PANI/graphene nanocomposites using a high-molecular weight PSS dopant and their application in H_2S detection, Nanoscale 6 (2014) 15181–15195, https://doi.org/10.1039/C4NR04413D.
[37] Z. Wu, X. Zong, Flexible and highly sensitive H_2S gas sensor based on in-situ polymerized SnO_2/rGO/PANI ternary nanocomposite with application in halitosis diagnosis, Sens. Actuators B Chem. 289 (2019) 32–41, https://doi.org/10.1016/j.snb.2019.03.055.
[38] T.T. Tung, J. Yoo, F.K. Alotaibi, M.J. Nine, R. Karunagaran, M. Krebsz, T. G. Nguyen, D.N.H. Tran, J.F. Feller, D. Losic, Graphene oxide-assisted liquid phase exfoliation of graphite into graphene for highly conductive film and electromechanical sensors, ACS Appl. Mater. Interfaces 8 (2016) 16521–16532, https://doi.org/10.1021/acsami.6b04872.
[39] C.K. Chua, M. Pumera, Monothiolation and reduction of graphene oxide via one-pot synthesis: hybrid catalyst for oxygen reduction, ACS Nano 9 (2015) 4193–4199, https://doi.org/10.1021/acsnano.5b00438.
[40] P. Liu, J. Yan, X. Gao, Y. Huang, Y. Zhang, Construction of layer-by-layer sandwiched graphene/polyaniline nanorods/carbon nanotubes heterostructures for high performance supercapacitors, Electrochim. Acta 272 (2018) 77–87, https://doi.org/10.1016/j.electacta.2018.03.198.
[41] D. Zhang, Z. Wu, P. Li, X. Zong, G. Dong, Y. Zhang, Facile fabrication of polyaniline/multi-walled carbon nanotubes/molybdenum disulfide ternary nanocomposite and its high-performance ammonia-sensing at room temperature, Sens. Actuators B Chem. 258 (2018) 895–905, https://doi.org/10.1016/j.snb.2017.11.168.
[42] R. Zeng, Z. Luo, L. Zhang, D. Tang, Platinum nanozyme-catalyzed gas generation for pressure-based bioassay using polyaniline nanowires-functionalized graphene oxide framework, Anal. Chem. 90 (2018) 12299–12306, https://doi.org/10.1021/acs.analchem.8b03889.
[43] R. Ghosh, A. Singh, S. Santra, S.K. Ray, A. Chandra, P.K. Guha, Highly sensitive large-area multi-layered graphene-based flexible ammonia sensor, Sens. Actuators B Chem. 205 (2014) 67–73, https://doi.org/10.1016/j.snb.2014.08.044.
[44] Z. Chen, A. Umar, S. Wang, Y. Wang, T. Tian, Y. Shang, Y. Fan, Q. Qi, D. Xu, L. Jiang, Supramolecular fabrication of multilevel graphene-based gas sensors with high NO_2 sensibility, Nanoscale 7 (2015) 10259–10266, https://doi.org/10.1039/c5nr01770j.
[45] Z. Yang, L. Guo, B. Zu, Y. Guo, T. Xu, X. Dou, CdS/ZnO core/shell nanowire-built films for enhanced photodetecting and optoelectronic gas-sensing applications, Adv. Opt. Mater. 2 (2014) 738–745, https://doi.org/10.1002/adom.201400086.
[46] X. Huang, N. Hu, R. Gao, Y. Yu, Y. Wang, Z. Yang, E. Siu-Wai Kong, H. Wei, Y. Zhang, Reduced graphene oxide-polyaniline hybrid: preparation, characterization and its applications for ammonia gas sensing, J. Mater. Chem. 22 (2012) 22488–22495, https://doi.org/10.1039/c2jm34340a.
[47] X. Tang, J.-P. Raskin, N. Kryvutsa, S. Hermans, O. Slobodian, A.N. Nazarov, M. Debliquy, An ammonia sensor composed of polypyrrole synthesized on reduced graphene oxide by electropolymerization, Sens. Actuators B Chem. 305 (2020) 127423, https://doi.org/10.1016/j.snb.2019.127423.
[48] Y. Yang, X. Yang, W. Yang, S. Li, J. Xu, Y. Jiang, Porous conducting polymer and reduced graphene oxide nanocomposites for room temperature gas detection, RSC Adv. 4 (2014) 42546–42553, https://doi.org/10.1039/c4ra06560c.
[49] J.N. Gavgani, A. Hasani, M. Nouri, M. Mahyari, A. Salehi, Highly sensitive and flexible ammonia sensor based on S and N co-doped graphene quantum dots/polyaniline hybrid at room temperature, Sens. Actuators B Chem. 229 (2016) 239–248, https://doi.org/10.1016/j.snb.2016.01.086.
[50] K.K. Saravanan, P. Siva Karthik, P.R. Mirtha, J. Balaji, B. Rajeshkanna, A one-pot hydrothermal-induced PANI/SnO_2 and PANI/SnO_2/rGO ternary composites for high-performance chemiresistive-based H_2S and NH_3 gas sensors, J. Mater. Sci. Mater. El. 31 (2020) 8825–8836, https://doi.org/10.1007/s10854-020-03417-4.
[51] F. Ahmadi Tabr, F. Salehiravesh, H. Adelnia, J.N. Gavgani, M. Mahyari, High sensitivity ammonia detection using metal nanoparticles decorated on graphene macroporous frameworks/polyaniline hybrid, Talanta 197 (2019) 457–464, https://doi.org/10.1016/j.talanta.2019.01.060.
[52] X. Chen, X. Xing, Z. Li, X. Zhao, Y. Tian, X. Lang, D. Yang, Three-dimensional porous carbon framework coated with polyaniline for highly stable and selective ammonia sensing, Sens. Actuators B Chem. 395 (2023) 134539, https://doi.org/10.1016/j.snb.2023.134539.
[53] X. Zhao, L. Lu, C. Xiang, Z. Huang, L. Sun, Y. Zou, Ammonia sensing using polyaniline composites by growth orientation control, ACS Appl. Nano Mater. 8 (2025) 17695–17703, https://doi.org/10.1021/acsanm.5c03301.
[54] L. Yang, L. Mao, S. Du, Z. Wang, W. Fu, C. Yao, L. Xu, H. Zhang, H. Cheng, Highly sensitive and fast response/recovery ammonia sensor based on PANI/LIG at room temperature, Sens. Actuators B Chem. 437 (2025) 137710, https://doi.org/10.1016/j.snb.2025.137710.

[55] Z. Guo, N. Liao, M. Zhang, W. Xue, Theoretical approach to evaluate graphene/PANI composite as highly selective ammonia sensor, Appl. Surf. Sci. 453 (2018) 336–340, https://doi.org/10.1016/j.apsusc.2018.05.108.
[56] S. Abdulla, T.L. Mathew, B. Pullithadathil, Highly sensitive, room temperature gas sensor based on polyaniline-multiwalled carbon nanotubes (PANI / MWCNTs) nanocomposite for trace-level ammonia detection, Sens. Actuators B Chem. 221 (2015) 1523–1534, https://doi.org/10.1016/j.snb.2015.08.002.
[57] F. Zeng, X. Liu, D. Diamond, K. Lau, Humidity sensors based on polyaniline nanofibres, Sens. Actuators B Chem. 143 (2010) 530–534, https://doi.org/10.1016/j.snb.2009.09.050.
[58] H. Liang, Y. Zhu, Z. Zhao, Z. Tang, Y. Niu, D. Zhang, Y. Wang, W. Gong, Enhanced room temperature ammonia gas sensing based on a multichannel PSS-functionalized graphene/PANI network, Analyst 150 (2025) 669, https://doi.org/10.1039/D4AN01488J.
[59] L. Kumar, I. Rawal, A. Kaur, S. Annapoorni, Flexible room temperature ammonia sensor based on polyaniline, Sens. Actuators B Chem. 240 (2017) 408–416, https://doi.org/10.1016/j.snb.2016.08.173.
[60] S. Liu, L. Shuai, Q. Zhu, L. Cao, F. Gu, L. Fan, S. Xiong, All-aerosol-jet-printed Fe^{3+} modified bilayers polyaniline flexible room temperature sensor with enhanced ammonia sensing properties, Talanta 287 (2025) 127684, https://doi.org/10.1016/j.talanta.2025.127684.